Journal of Applied Polymer Science

In situ synthesis of polystyrene nanocomposites with layered double hydroxide with an unusual anion arrangement: Morphology and thermal and mechanical properties

Rodrigo Botan, Telma Regina Nogueira Caio, Liliane Maria Ferrareso Lona
School of Chemical Engineering, University of Campinas, Campinas São Paulo, Brazil
Correspondence to: R. Botan (E-mail: botan.03@gmail.com)

ABSTRACT: Today, the steady advance of technology and society makes the development of materials with improved properties of paramount importance. In this article, we contribution to this area by presenting an *in situ* bulk synthesis of polystyrene (PS) nanocomposites with layered double hydroxide (LDH) as a reinforcement. The LDH that we adopted presented an unusual arrangement of anions and had ZnAl cations intercalated with laurate and palmitate anions. The nanocomposites were analyzed by X-ray diffraction and transmission electron microscopy to characterize their morphologies. The thermal properties, including the glass-transition temperature and thermal stability, were measured by differential scanning calorimetry and thermogravimetric analysis, respectively. The mechanical properties and flexural fracture morphologies were also determined, with a bending test. The results demonstrate that the synthesized nanocomposites showed considerable improvements in their thermal stability and mechanical properties compared with the neat PS. © 2015 Wiley Periodicals, Inc. J. Appl. Polym. Sci. **2016**, *133*, 42856.

KEYWORDS: clay; nanostructured polymers; properties and characterization; synthesis and processing; thermogravimetric analysis (TGA)

Received 12 May 2015; accepted 21 August 2015
DOI: 10.1002/app.42856

INTRODUCTION

The quest for the synthesis, development, and characterization of new polymer nanocomposites has shown a steady and significant increase.[1–4] This quest is mainly due to the remarkable improvements in nanocomposite properties when compared with neat polymers or conventional microcomposites and macrocomposites using low levels of reinforcements, usually a maximum of 5 wt %. These mainly include improvements in the mechanical, thermal, flammability, and physical properties.[1–6]

Among the many existing polymer nanocomposite types, the ones synthesized with layered double hydroxides (LDHs) have been highlighted, mainly because of the great versatility that these LDHs present in their synthesis and the properties of the new polymer nanocomposites.[7–9] However, one difficulty that is encountered in the use of LDHs in polymer nanocomposite synthesis is their higher tunable charge density on layers; this cause stronger interaction among the hydroxide layers and hinders the adsorption of monomers or polymers between these layers and consequently the synthesis of polymer nanocomposites with better morphologies and properties.[3,7–9]

In an effort to overcome this high charge density, research groups have used different anions in LDHs with the primary purpose of synthesizing polymer/LDH nanocomposites with improved morphologies and properties.[1–6,9] Most researchers have presented sodium dodecyl sulfate as an anion;[3,10,11] these studies include some by our research group.[1,12,13] Other researchers have presented carboxylates,[14,15] dodecyl benzenosulfonate,[16] bis(2-ethylhexyl) phosphate,[16] and others[2,8,17] as anions.

Among the several anions types used in LDHs to synthesize polymer nanocomposites with better morphologies and properties, carboxylates have been shown to produce the best results; nevertheless, the search for better results and advances in the state of the art are still needed.[14,15,18] In pursuit of this improvement, the use of LDHs with unusual anion arrangements for polymer nanocomposite synthesis have been presented as an alternative. LDHs with unusual anion arrangements are obtained when they are synthesized with carboxylate anions, and these anions are used in excess, as reported in articles that focus on the LDH synthesis and characterization.[19–21] With the use of this anion arrangement, it is possible to synthesize LDHs with higher basal spacing; this decreases the effect of the higher charge density and enables the synthesis of nanocomposites with better morphologies and properties.[19–22]

However, despite the possibility of the synthesis of polymer nanocomposites with improved morphologies and properties with LDHs with unusual anion arrangements, we found no reports or papers in the literature. Thus, in this study, we aimed to synthesize and characterize nanocomposites of polystyrene (PS)/LDH with unusual anion arrangements, investigating whether this unusual structure of LDHs provided better morphologies and thermal and mechanical properties when compared to the neat PS and PS/LDH nanocomposites reported in the literature. In this study, we also investigated the influence of different anions [laurate (L) and palmitate (P)] on the synthesis, morphologies, and properties of PS/LDH nanocomposites. The nanocomposites were produced with three different compositions of LDH (0.5, 1, and 2 wt %) and characterized by X-ray diffraction (XRD), transmission electron microscopy (TEM), differential scanning calorimetry (DSC), thermogravimetric analysis (TGA), and a bending test. The flexural fracture morphologies were obtained with scanning electron microscopy (SEM).

Another important point in this study was the synthesis route that we used (*in situ*). When compared to other routes, the *in situ* synthesis presented better control and a more homogeneous distribution of LDHs in the polymer matrix. For nanocomposites synthesized via melt blending, for example, it is notoriously difficult to achieve a homogeneous distribution of nanometer-scale particles in a highly viscous polymer melt, and the aggregation of the particles cannot be prevented.[23,24]

Thus, as shown by the development of this study, the nanocomposite synthesis of PS/LDH with unusual anion arrangements presented important improvements in the morphology and thermal and mechanical properties.

EXPERIMENTAL

Materials

Lauric acid ($C_{12}H_{24}O_2$) and palmitic acid ($C_{16}H_{32}O_2$; Vetec), zinc chloride ($ZnCl_2$; Ecibra), aluminum chloride ($AlCl_3$; Synth), and sodium hydroxide (NaOH; Fmaia), all analytical grade, were used for the LDH synthesis.

For the nanocomposite synthesis, NaOH (Fmaia), calcium chloride ($CaCl_2$; Ecibra) and styrene monomer with 99% purity and a *tert*-butylperoxy-2-ethylhexyl carbonate initiator (Sigma-Aldrich Co.) were used.

Preparation of the LDHs

The LDHs were synthesized with the coprecipitation method[20,25,26] with some modifications. For the LDH synthesis, $C_{12}H_{24}O_2$ or $C_{16}H_{32}O_2$ in excess (132 mmol) and deionized/degassed water were added to the reactor and stirred for 15 min. After that, NaOH and deionized/degassed water formed an alkaline solution and were added to the reactor, with the aim of keeping the pH of reaction constant at around 9–10. The salt solution, which consisted of $ZnCl_2$ (66 mmol) and $AlCl_3$ (33 mmol) in 200 mL of deionized/degassed water, was slowly added.

The reaction was stirred for 7 h and stored for 12 h so the LDH crystals would ripen. The synthesis was carried out in a nitrogen atmosphere to avoid the presence of CO_2 from the air at controlled temperature (35°C) and at a pH of around 9–10. CO_2 should be avoided because it competes in the LDH intercalation with L or P anions.

Subsequently, the material was centrifuged, extensively washed with deionized/degassed water, dried at 50°C *in vacuo,* and sieved to a particle size of 0.152 mm (100 mesh).

Preparation of the PS Nanocomposites

The nanocomposites were produced by *in situ* free-radical bulk polymerization. Neat PS was also synthesized to compare the results. The nanocomposites were composed of PS/LDH intercalated with L or P (PS/ZnAl–L and PS/ZnAl–P) at different loadings of LDH (0.5, 1, and 2% w/w).

First, monomer purification was carried out[27] because the monomer used in this study contained an inhibitor. The monomer was washed thrice with a 10% w/v NaOH solution, washed thrice with deionized water, and dried over $CaCl_2$.

For the polymerization of neat PS, the styrene monomer and initiator (*tert*-butylperoxy-2-ethylhexyl carbonate at a concentration of 36 mmol/L) were used, and for the nanocomposite production, in addition to these two compounds, LDH was added. Desired quantities of the monomer, initiator, and LDH (0.5, 1, or 2% w/w) were weighed, mixed, and then placed into glass ampules. In the nanocomposite synthesis, LDH and styrene were mixed and stirred for 75 min before the addition of the initiator. These ampules were degassed by at least three freeze–pump–thaw cycles *in vacuo* to remove oxygen. After torch sealing, the ampules were placed into an oil bath at a controlled temperature (108°C) for 210 min.[12,13] After polymerization, the ampules were broken, and the samples were stored for later analysis.

Analyses Used for Characterization

XRD was performed with a Shimadzu XRD 7000 instrument. This instrument used a copper cathode with wavelength of 1.5406 Å, a generator tension of 40 kV, and a current of 30 mA. Scans were taken in a 2θ range of 1.5–70° with a 2°/min step size.

Fourier transform infrared (FTIR) spectroscopy was performed with a PerkinElmer instrument in the region 4000–450 cm^{-1} with the KBr method.

An SEM instrument (LEO model 440i) was used with the primary purpose of observing the LDH morphologies and the failure surfaces after the bending test.

TEM was performed in a JEOL JEM 3010 instrument with an acceleration voltage of 300 kV. The samples were ultramicrotomed with a glass knife to give 120 nm thick slices. The slices were collected in water at room temperature.

TGA measurements were performed on a TA Instruments model TGA 2050 instrument. The experiments were conducted under an oxidant atmosphere (flow rate = 100 mL/min) at a scan rate of 10°C/min and in the temperature range 25–700°C. The TGA samples were analyzed in duplicate, and the resulting variation was ±3°C.

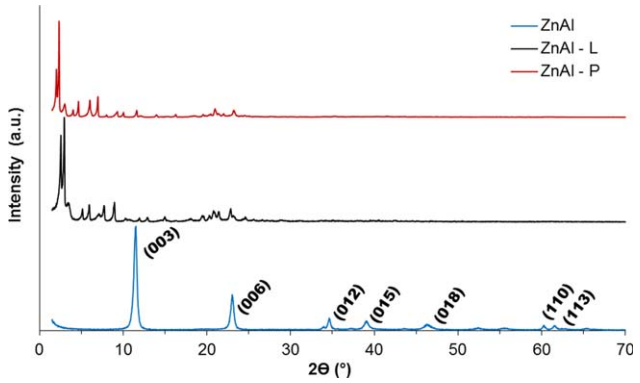

Figure 1. XRD patterns for the modified and unmodified LDHs. [Color figure can be viewed in the online issue, which is available at wileyonlinelibrary.com.]

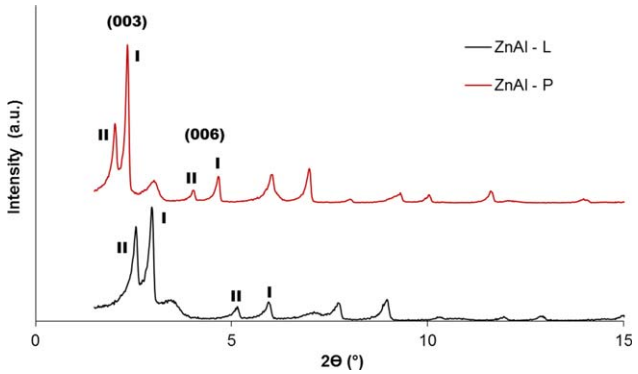

Figure 2. XRD patterns at a low angle to ZnAl–L and ZnAl–P. [Color figure can be viewed in the online issue, which is available at wileyonlinelibrary.com.]

A DSC instrument (Mettler-Toledo model FP85) was used for DSC analysis. The conditions used for the analyses were an inert atmosphere (nitrogen flow rate = 50 mL/min) with a heating rate of 20°C/min at temperatures from 35 to 180°C.

The mechanical test carried out in this study was the three-point bending test, and it was performed according to ASTM D 790[28] to obtain the flexural strength, modulus, and strain at break of the materials. However, because of the small amount of material obtained by the *in situ* polymerization, three specimens were used for each composition of synthesized materials. Specimens with dimensions of 64 × 12.7 × 3.15 mm^3 were fabricated by injection into a mini-injector (Thermo Fisher Scientific, Haake MiniJet II). In these trials, a mechanical universal testing machine was used (model MTS 810). The strain rate used in this test was 0.01 mm/mm/min.

RESULTS AND DISCUSSION

LDH

The first materials synthesized in this study were the LDHs formed by ZnAl–L and ZnAl–P. These materials were characterized by XRD, FTIR spectroscopy, and SEM to identify their structure and morphologies.

Figure 1 shows XRD patterns for the two synthesized LDHs. Also shown in this figure is the XRD pattern of LDH (ZnAl) without modification and with chloride anions.

As shown in Figure 1, the ZnAl pattern without modification presented a characteristic regular series of basal diffraction peaks, and through calculation of the basal spacing by Bragg's diffraction law, we obtained a value of 7.74 Å.[19,20,29,30]

Analyzing the ZnAl patterns intercalated with the anions L and P (ZnAl–L and ZnAl–P, respectively) and comparing them with the ZnAl pattern without modification, we observed the same characteristic series of basal diffraction peaks with a displacement of the peaks to lower values of 2θ and a lower crystallinity. These facts suggest the effective syntheses of ZnAl intercalated with L and P anions.[19–21]

However, the ZnAl–L and ZnAl–P patterns also showed the formation of an additional series of basal diffraction peaks, which are shown in greater detail in Figure 2, in which the patterns are presented to a value of up to 15° (2θ). This new series of basal diffraction peaks occurred when excess anion was used in the LDH synthesis, as done in this study.

This unusual anion arrangement for LDHs has been reported in some studies,[19,25,26] including in the studies of Xu and Braterman[20] and Kuehn and Porllmann.[21] In this structure of unusual anion arrangements, the existence of two types of anion arrangements, represented by the two series of basal diffraction peaks found in the XRD patterns, is suggested. The first and most common arrangement is one in which molecules of these anions are aligned uniformly in unitary form at a certain angle in the interlayer spacing; this is defined as a monolayer (presented in the patterns as *I*).[19–21,25,26] The second arrangement occurs when molecules of these anions in the interlayer spacing are stacked in pairs at a certain angle; this is defined as a bilayer (presented in the patterns as *II*). Monolayer and bilayer models were observed in some studies presented in the literature.[19,20,26]

Thus, the formation of these structures, especially the bilayer, allows an LDH synthesis with higher basal spacing; this decreases the effect of the higher charge density, consequently improves the likelihood of monomer/polymer adsorption in the

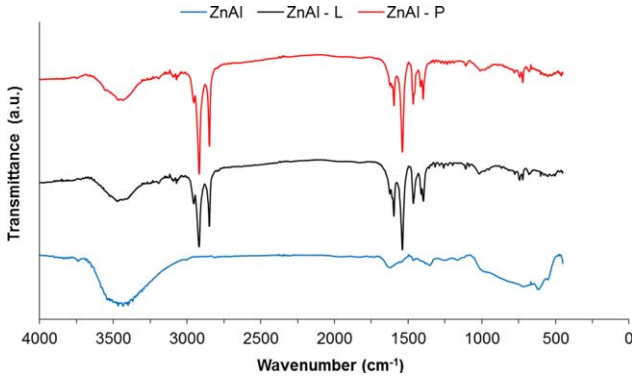

Figure 3. FTIR spectra for ZnAl without modification, ZnAl–L, and ZnAl–P. [Color figure can be viewed in the online issue, which is available at wileyonlinelibrary.com.]

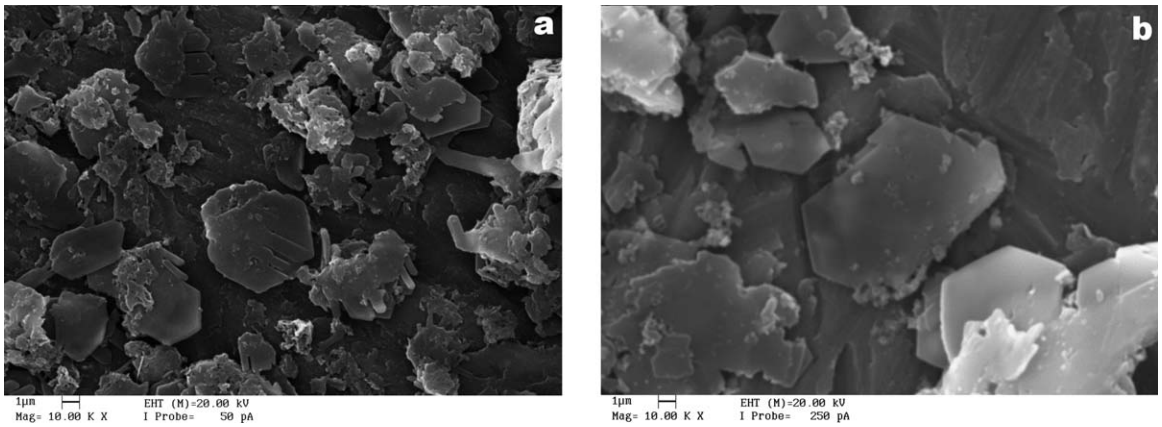

Figure 4. Morphology of (a) ZnAl–L and (b) ZnAl–P as determined by SEM.

interlayer spacing, and allows the synthesis of nanocomposites with improved morphologies and properties.

Through the XRD patterns and Bragg's diffraction law, the basal spacing values for the synthesized LDHs were calculated. That of the ZnAl–L monolayer was 29.80 Å, and that of the bilayer was 34.46 Å. For the ZnAl–P monolayer, the value was 37.76 Å, and for the bilayer, it was 44.14 Å. The results obtained show a considerable expansion in the basal spacing when compared to that of the unmodified ZnAl because the basal spacing value for this material was 7.74 Å. This was a further indication of the effective intercalation of ZnAl with L and P.

After characterization by XRD, the next technique used was FTIR spectroscopy, with the main objective being to characterize the chemical bonds (key functional groups) of these materials and complement the information obtained by XRD. Figure 3 shows the FTIR spectra of the ZnAl without modification and ZnAl–L and ZnAl–P.

The unmodified ZnAl spectrum, as widely known, presented a band in the region 3800–3100 cm^{-1}; this resulted from the superposition of the OH stretching vibrations present in the water molecules and the hydroxide layer. Around 1673 cm^{-1}, another band related to the bending vibrations of water molecules was found, and in the region 830–450 cm^{-1}, the characteristic M—O or O—M—O (where M is Zn or Al) lattice vibration bands were observed.[20,31,32] In this spectrum, a light band around 1386 cm^{-1} was also identified; it corresponded to contamination by carbonate anions during the synthesis.[20,31]

When the ZnAl–L and ZnAl–P spectra were analyzed, it was possible to identify bands that were not found in the unmodified ZnAl spectrum. These bands were related to the intercalated L and P anions and were observed at 3000–2800 cm^{-1}; this corresponded to the symmetric and asymmetric stretching vibrations of the CH group. We also observed bands related to the bending vibrations of CH_2 and CH around 1467 and 720 cm^{-1}, respectively, and bands identified as the asymmetric and symmetric stretching vibrations of COO at 1544 and 1410 cm^{-1}, respectively.[1,15,19,20]

Other bands at 1595 and 1399 cm^{-1} were observed in the ZnAl–L and ZnAl–P spectra. These bands were identified as the asymmetric and symmetric stretching vibrations, respectively, of the COO group in COOH.[19,20] The existence of these bands corroborated with the results found by XRD. They are only reported in LDH spectra when there is the formation of an unusual arrangement of anions.[20]

In addition to the bands identified in the ZnAl–L and ZnAl–P spectra, which were related to intercalated anions, bands were also observed around 3500 cm^{-1}, related to the stretching vibrations of OH in the hydroxide layer, and in the region 662–552 cm^{-1}, related to the lattice vibration of M—O or O—M—O.[1,15,19,20]

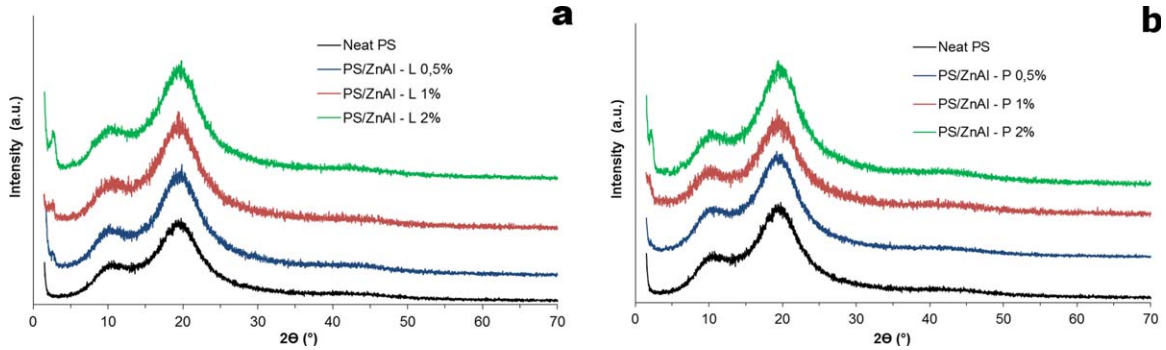

Figure 5. XRD patterns for the nanocomposites formed by (a) PS/ZnAl–L and (b) PS/ZnAl–P. [Color figure can be viewed in the online issue, which is available at wileyonlinelibrary.com.]

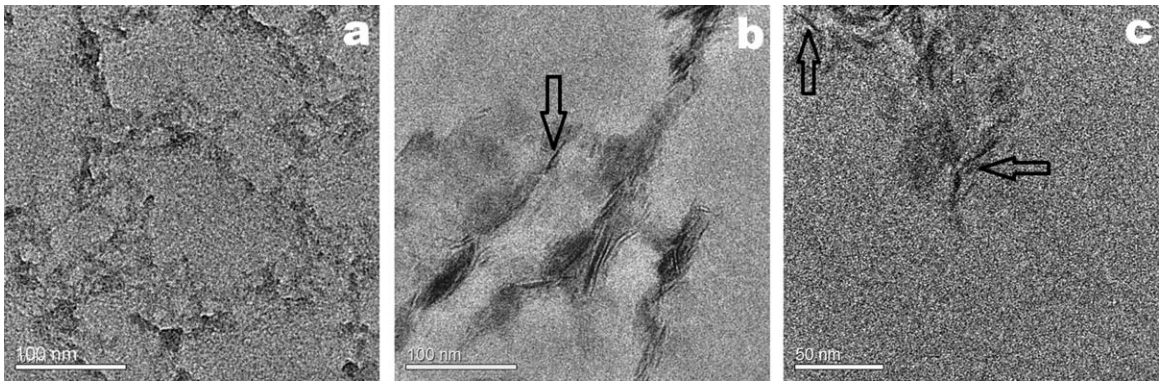

Figure 6. TEM images obtained for the PS/LDH synthesized nanocomposites: (a) nanocomposite formed with PS/ZnAl–P 2%, (b) nanocomposite formed with PS/ZnAl–L 2%, and (c) nanocomposite formed with PS/ZnAl–P 1%.

For a complete morphological and structural characterization of the synthesized LDHs, SEM was used. Figure 4 shows the images obtained by SEM.

It is very well known that unmodified LDHs (natural or synthetic) have a hexagonal platelike morphology with lateral dimensions from 50 nm to a few micrometers.[19,20] However, when these LDHs are synthesized with organic anions (carboxylate), the interactions that occur between these anions and cations during synthesis cause some changes in the crystal shape.[19–21,25,26] This differentiation in the crystal shape was observed in the SEM images (Figure 4), which showed a hexagonal plate not well characterized or defined and with incomplete shaping and rounded corners. This structure is defined as a platelike particle, and it is characteristic of LDHs with the kinds of anions used in this study.[19–21,25,26] The average values found for the lateral dimensions of the LDHs were 3.23 μm for ZnAl–L and 7.54 μm for ZnAl–P.

In summary, the synthesized LDHs showed strong evidence to suggest the effective synthesis of these materials intercalated with the L and P anions. These LDHs also presented unusual anion arrangements, which could enable their use as reinforcements in the synthesis of PS nanocomposites with better morphologies and properties.

Structure and Morphologies of the PS/ZnAl–L and PS/ZnAl–P Nanocomposites

After the synthesis and characterization of LDHs, the next step of this study was the synthesis and characterization of the neat PS and PS nanocomposites. For the structural and morphological characterization of these materials, XRD and TEM analysis were performed.

Figure 5 shows the XRD patterns for the neat PS and PS/ZnAl–L and PS/ZnAl–P nanocomposites. The nanocomposites were synthesized with 0.5, 1, and 2% LDHs. The main objective of the nanocomposite XRD analysis was to provide indications of how the reinforcing material was distributed and structured in the polymer matrix.

The nanocomposite XRD patterns, with an overall similarity to the polymer matrix pattern and no peak corresponding to crystalline material (reinforcement), even at lower values of 2θ, suggested that the nanocomposite had an exfoliated structure or disordered immiscible structure.[12,16,17] This structure (exfoliated) represented the breaking of the layered structure of the reinforcement, and this resulted in random layer distribution in the polymer matrix. However, when the nanocomposite XRD patterns showed the formation of small peaks at low values of 2θ, any kind of organizational reinforcement remained in the polymer matrix; this suggested the formation of an intercalated morphology. In an intercalated morphology, the adsorption of the monomer into the interlayer space usually occurs; however, a complete layered structure breakdown does not occur.[12,16,17]

Importantly, the conclusions obtained from the analysis of the nanocomposite XRD patterns were just indications, and it was of great importance to use other tools, usually TEM, for the

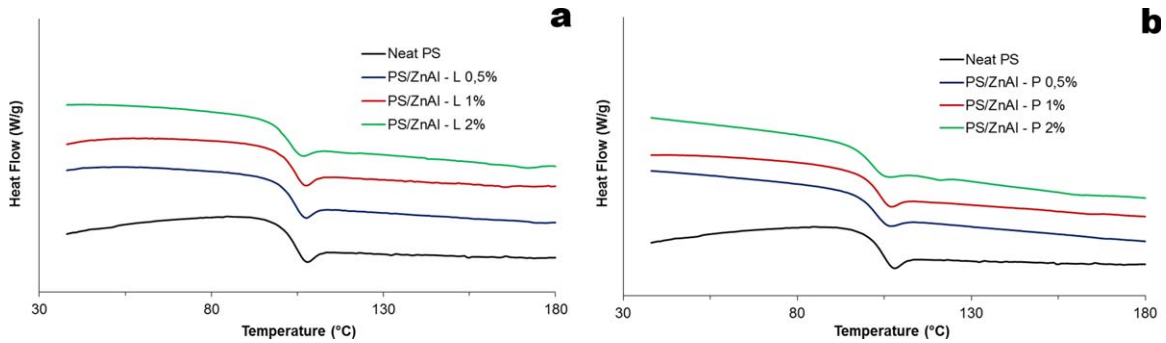

Figure 7. DSC curves for the neat PS and nanocomposites formed with (a) PS/ZnAl–L and (b) PS/ZnAl–P. [Color figure can be viewed in the online issue, which is available at wileyonlinelibrary.com.]

Table I. Values of the Glass-Transition Temperatures Obtained by DSC for the Neat PS and Nanocomposites

Material	Glass-transition temperature (°C)
Neat PS	103
PS/ZnAl-L 0.5%	103
PS/ZnAl-L 1%	103
PS/ZnAl-L 2%	102
PS/ZnAl-P 0.5%	101
PS/ZnAl-P 1%	101
PS/ZnAl-P 2%	100

Table II. Summary of the TGA Data for the Neat PS and Synthesized Nanocomposites

	Temperature (°C)		
Material	T_{ons}	T_{ha}	T_{end}
Neat PS	299	332	363
PS/ZnAl-L 0.5%	310	348	377
PS/ZnAl-L 1%	320	356	384
PS/ZnAl-L 2%	324	355	380
PS/ZnAl-P 0.5%	312	352	381
PS/ZnAl-P 1%	319	357	386
PS/ZnAl-P 2%	327	359	383

confirmation and identification of the morphology. Nevertheless, it is important to know that the XRD patterns of the nanocomposites with small amounts of reinforcements, up to 1 wt %, sometimes did not show any peak because of the equipment detection limit.

In the analysis of the neat PS pattern, we observed the existence of two small halos centered at approximately 10 and 20° (2θ); these were due to the amorphous nature of this polymer.[12,13,23] In the analysis of the XRD patterns of the synthesized nanocomposites, we observed that, independent of the LDHs used in equal compositions, their patterns were, in general, very similar.

The nanocomposites with 0.5% LDHs presented XRD patterns identical to those of the neat PS with no peak, even at low 2θs. The nanocomposites with 1% LDHs had a slight bias at low 2θs; this suggested the beginning of the peak formation related to some organization of LDHs in the polymer matrix. The nanocomposite with 2% LDHs exhibited peaks at low 2θs; this suggested the formation of an intercalated morphology.

To identify the nanocomposite morphologies and step up the results obtained by XRD, TEM analyses were performed. TEM image analysis with a low magnification usually shows an overall distribution of reinforcement in the polymer matrix, whereas analysis with high magnifications show details (single layers or few layer aggregates) of their reinforcement.[12,13,16,33]

Figure 6 shows the images obtained by TEM at low and high magnifications. It is important to note that the TEM analyses for all of the synthesized nanocomposite in all of the compositions were not able to identify a significant difference, so the selected images represent the results obtained for all of the nanocomposites.

The first TEM image, shown in Figure 6(a), is a low-magnification image. In this image, the dark lines and spots represent the LDH, and the major part, in gray, represents the polymer matrix. Through this image, it was possible to suggest that the synthesized nanocomposites showed a satisfactory overall distribution of LDH in the PS matrix.

Figure 6(b) shows a high-magnification image. With this image, it was possible to suggest the existence of an intercalated morphology in the nanocomposites. Layers aligned with a small section of the polymer in its interlayer spacing were observed, but in this image, it was also possible to identify the exfoliated layers form (black arrow); this demonstrated that they coexisted with mainly intercalated structures with some points of exfoliated structure. Figure 6(c) confirms the existence of exfoliated layers with a high-magnification image (50 nm). The exfoliated layers are identified in the figure by the black arrows.

Thus, the TEM analysis suggested that the nanocomposites in all of the compositions showed a mixture of structures; the main and largest amount was intercalated and coexisted with small portions of exfoliated material, so the structure of these nanocomposites was defined as intercalated/exfoliated.

When comparing the results obtained by XRD and TEM together, we observed that both corroborated with the intercalated/exfoliated morphology that we found, in particular for the

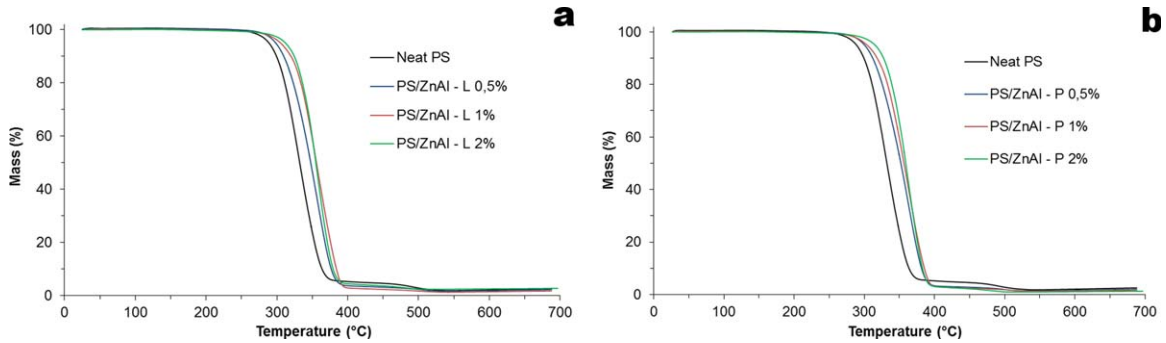

Figure 8. TGA curves for the neat PS and nanocomposites formed with (a) PS/ZnAl–L and (b) PS/ZnAl–P. [Color figure can be viewed in the online issue, which is available at wileyonlinelibrary.com.]

Table III. Flexural Strength and Strain at Break Values for the Neat PS and Nanocomposites

Material	Flexural strength (MPa) (%)	Strain at break (%)
Neat PS	20.62 ± 3.59	0.65 ± 1.51
PS/ZnAl-L 0.5%	23.51 ± 4.09	0.73 ± 2.67
PS/ZnAl-L 1%	25.18 ± 8.39	0.78 ± 8.33
PS/ZnAl-L 2%	33.30 ± 6.25	1.02 ± 6.62
PS/ZnAl-P 0.5%	24.90 ± 9.12	0.77 ± 9.02
PS/ZnAl-P 1%	28.41 ± 4.37	0.88 ± 3.53
PS/ZnAl-P 2%	32.17 ± 8.57	0.99 ± 7.61

nanocomposites with 1 and 2% LDHs because XRD peaks were identified that suggested some organization of the LDHs in the PS matrix. As for the nanocomposites with 0.5% LDHs, the lack of an XRD peak was mainly due to the low concentration.

The results for the synthesized nanocomposite morphology in this study is a step forward because studies reported in the literature that have used PS/LDHs have mostly featured immiscible or microcomposite morphologies.[14,16,34]

Study of the Thermal Properties

In this study, the thermal properties of the nanocomposites were obtained by DSC and TGA.

The DSC analysis was conducted with the main objective of defining the nanocomposites' glass-transition temperatures and comparing them with those of the neat PS. The glass-transition temperature is a parameter of fundamental importance for further nanocomposite processing.

As shown in Figure 7 (DSC curves), the neat PS and nanocomposites in all compositions and percentages showed very similar behaviors.

The obtained glass-transition temperature values for the neat PS and nanocomposites are shown in Table I.

With the analysis and comparison of the results of the glass-transition temperature, it was possible to identify a slight decrease in these values with increasing LDH percentage; however, this reduction was considered very low, not exceeding 3°C (for the PS/ZnAl–P nanocomposite with 2% LDH).

Comparing anions L and P, we observed that when P anions were used, the glass-transition temperature was slightly lower.

However, it was possible to suggest, even with the trend, that no significant changes in the glass-transition temperatures were observed among the two kinds of nanocomposites and neat PS.

The thermal stability is a very important property in many applications for the polymer materials, and this property was measured by TGA. Figure 8 shows the curves of the TGA, and Table II shows the data obtained from the curves.

The specific values in the curves of Figure 8 were analyzed. The first analysis was the point of onset degradation temperature (T_{ons}), defined as the temperature where the polymer starts to degrade, and in the TGA curve, it was obtained when 10% of the material was degraded. The second point was the half-degradation temperature (T_{ha}), defined as the temperature where the half-degradation of the polymer occurs, and in the TGA curve, it was obtained when 50% of the material was degraded. The third point was the end degradation temperature (T_{end}), defined as the temperature where almost all the material has been degraded, and in the TGA curve, it was obtained when 90% of the material was degraded.

The neat PS, as shown, presented a characteristic behavior in this assay. This material began to degrade, or lose weight, at a temperature around 300°C, and from this point, the PS polymer chains degraded to values of temperature around 380°C, that is, a temperature at which almost the entire material was consumed.[13,18,24]

When the TGA curves were compared, it was possible to identify the same standard for the nanocomposites and neat PS; however, in all of the synthesized nanocomposites, a slower degradation occurred. For example, for PS/ZnAl–L 2%, there was a gain of 25°C for T_{ons} and a gain of 23°C for T_{ha}, and for PS/ZnAl–P 2%, the gains were 28 and 27°C for T_{ons} and T_{ha}, respectively.

These results in thermal stability are very promising, especially when compared with those reported in the literature. In previous studies developed by our group with other LDH types, the results obtained for the reinforcement ratio of 2% show an average gain of 10°C.[12,13] In other studies reported in the literature with PS/LDH modified with carboxylate anions,[14] on average, the gain in T_{ha} was 15°C for nanocomposites with 3% LDH.

The improvement in the thermal stability found in this study was attributed to the considerable increase in the basal spacing of LDH; this led to an improvement in the physical interactions between the polymer and layers of LDH. With these interactions, the material exhibited greater resistance to the diffusion of oxygen and volatile compounds, and this contributed to a slower degradation.[7,13–15,24]

Mechanical Properties

The determination of the mechanical properties for polymer nanocomposites has great importance because many applications for these nanocomposites depend on their mechanical properties.[1,22,35] Despite this great importance, studies of

Table IV. Flexural Modulus of the Neat PS and Nanocomposites at Different Loadings

Material	Flexural modulus (Mpa) (%)	Modulus/modulus PS ratio
Neat PS	3.186 ± 0.81	1.000
PS/ZnAl-L 0.5%	3.214 ± 0.69	1.009
PS/ZnAl-L 1%	3.234 ± 0.86	1.015
PS/ZnAl-L 2%	3.247 ± 0.89	1.019
PS/ZnAl-P 0.5%	3.227 ± 0.89	1.013
PS/ZnAl-P 1%	3.235 ± 1.14	1.015
PS/ZnAl-P 2%	3.240 ± 1.00	1.017

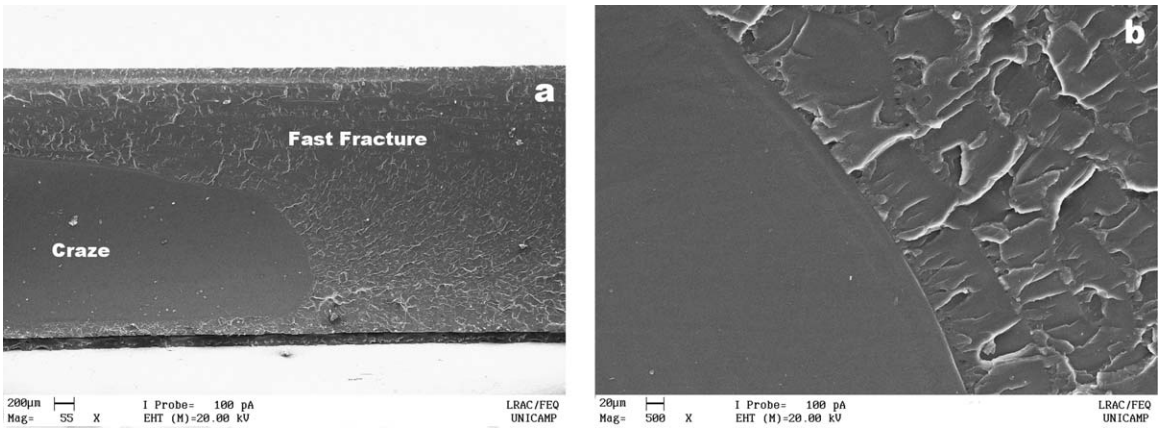

Figure 9. (a) Image analysis of neat PS fracture obtained by SEM and (b) focus on the transition from the craze region to the brittle fracture region.

mechanical properties of PS/LDH nanocomposites are still scarce.

The mechanical properties of the materials synthesized in this study were obtained through the three-point bending test. The bending test was chosen because of the fragility of the neat PS and its nanocomposites, which makes tensile test results unreliable.

Through the bending test, the flexural strength and strain at break were obtained. The results are shown in Table III. The flexural modulus was also obtained and is shown in Table IV. For these bending tests, three specimens were used for each composition of the synthesized materials. Thus, the values represent the average with the percentage deviation, which was calculated with the following equation:[36]

$$\text{Percentage deviation} = (\text{Measured value} - \text{Average})/\text{Average} \times 100\%$$

We observed from the results that all of the nanocomposites in all of the compositions showed a tendency of increase in the flexural strength and strain at break values compared to the neat PS. These nanocomposites also showed another tendency: an increase in the LDH amount resulted in an increase in the values of the two properties. The different nanocomposites showed very similar behavior and results, so the discussion is similar for both cases.

Comparing the results of the flexural strength obtained for the neat PS and nanocomposites with 0.5% reinforcement, we found that the nanocomposites had, on average, 18% higher values. These values for the nanocomposite with 1% reinforcements increased to 30%; for the nanocomposites with 2% reinforcements, there was an average increase of 58%. The strain at break also showed average improvements of 15, 28, and 54% for the nanocomposites with 0.5, 1, and 2% LDHs, respectively.

These results demonstrate that the synthesized nanocomposites showed a tendency of gains in the mechanical properties when compared to the neat PS. These gain could have been due to the large contact surface area between the LDHs and PS. Because of the greater contact area, the polymer chain mobility was difficult, and the LDHs acted as a barrier to the chain movement and helped stabilize the crack growth; this enhanced its mechanical properties.[3,14,35–37]

The flexural modulus, as well as flexural strength, and strain at break of the nanocomposites (Table IV) also improved compared with the neat PS.

The results in the mechanical properties obtained for these synthesized nanocomposites represent an advance for this class of materials because among the few studies in literature that examine the mechanical properties, there was no improvement in

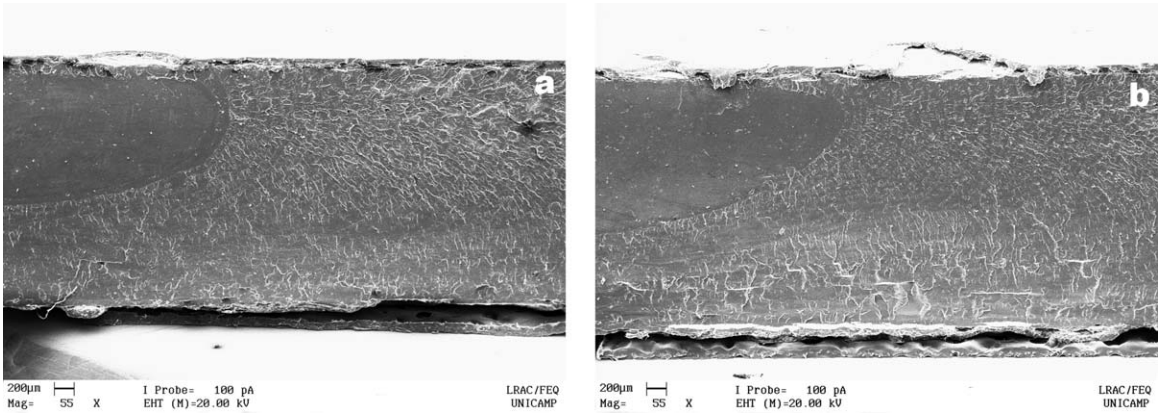

Figure 10. Fracture image analysis obtained by SEM for (a) PS/ZnAl–L 2% and (b) PS/ZnAl–P 2%.

these properties, and in some cases, these properties became worse.[14,18]

Flexural Fracture Analysis

To understand the results obtained in the mechanical properties of the synthesized nanocomposites, flexural fracture analyses were performed.

The fracture or breakage of the material is the separation into two or more pieces in response to a request. Briefly, materials science classifies fractures into two types: brittle (fast) or ductile. Brittle fracture happens when materials break before plastic deformation occurs, whereas the ductile fracture is characterized by the existence of yielding and, consequently, plastic deformation before the rupture of the material.[38]

In the study of the neat PS flexural fracture, it was possible to identify two distinct regions, which were the craze and fast fracture regions, as shown in Figure 9.

The main fracture mechanism of neat PS was crazing. This mechanism can be defined as localized yielding and fracture initiation. When the material suffers a certain tension, small cracks (voids) are formed, which produce the initial real crack. However, instead of the small cracks coalescing to form a real crack, these small cracks are stabilized by fibrils of oriented polymer material.[36,39]

Thus, this material fracture started with a crazing mechanism. From the moment that the fibrils could not stabilize, small cracks and real cracks were formed, and the material underwent a fast fracture until it reached breaking. Such a transition was well identified in the fracture analysis.

Comparing the fracture of the neat PS and all of the nanocomposites, we identified no significant differences, beginning from the fracture by crazing up to fast fracture until their breakup. Figure 10 shows the fractures images of the nanocomposites synthesized with the highest reinforcement proportion (2%).

The nanocomposites and neat PS showed basically the same fracture mechanism; however, the mechanical properties obtained for the nanocomposites were higher than those of the neat PS. Therefore, it is possible to suggest that some differentiation occurred in the crazing stage.

At the crazing stage, there was crack stabilization through the fibrils of the polymer material so that the material could bear a particular request until it passed to the fast fracture and then to the disruption. At this stage, the nanocomposites probably stabilized small cracks with greater efficiency and, consequently, withstood higher requests than the neat PS.[36,39]

This greater stability for the nanocomposites might have been due to the existence of distributed nanometer-scale layers in the polymer matrix, which acted as barriers to movements, and the coalescence of small cracks, as well as fibrils; this made these materials support larger amounts of requests.[36,37,39]

CONCLUSIONS

In this work, PS/LDH nanocomposites were successfully synthesized. These LDHs were formed by ZnAl cations and L and P anions, with unusual anion arrangements. These nanocomposites showed a mixture of morphology, mainly intercalated with a few parts exfoliated; this suggested an intercalated/exfoliated morphology. The thermal properties of the nanocomposites demonstrated an improvement in the thermal stability compared to that of the neat polymer. An average improvement of 25°C was obtained for nanocomposites with 2% reinforcements when 50% of the materials were degraded. The mechanical properties, measured by the bending test, showed an increase, with an average 58% improvement in the flexural strength for the nanocomposites with higher reinforcement percentages. Through fracture analysis, it was possible to suggest that this improvement in the mechanical properties was due to the existence of distributed nanometer-scale layers in the polymer matrix, which acted as barriers to movement, and the coalescence of small cracks. When the PS/LDH nanocomposites synthesized with L and P anions were compared, considerable differences were not identified in all of the characterization techniques used. Thus, it is possible to suggest that PS/LDH nanocomposite synthesis with unusual anion arrangements presents an innovative approach and allowed the production of nanocomposites with improved thermal and mechanical properties.

ACKNOWLEDGMENTS

The authors acknowledge Coordenação de Aperfeiçoamento de Pessoal de Nivel Superior and Fundação de Amparo à Pesquisa do Estado de São Paulo for their financial support and the Brazilian National Laboratory for Synchrotron Light (Laboratório Nacional de Luz Síncrotron) for the use of microscopes and its dependencies.

REFERENCES

1. Nogueira, T.; Botan, R.; Wypych, F.; Lona, L. *J. Appl. Polym. Sci.* **2012**, *124*, 1764.
2. Guo, B. Z.; Zhao, Y.; Huang, Q. T.; Jiao, Q. Z. *Compos. Sci. Technol.* **2013**, *81*, 37.
3. Peng, H.; Tjiu, W. C.; Shen, L.; Huang, S.; He, C.; Liu, T. *Compos. Sci. Technol.* **2009**, *69*, 991.
4. Neto, J. C. M.; Botan, R.; Lona, L. M. F.; Neto, J. E.; Pippo, W. A. *Polym. Bull.* **2015**, *72*, 387.
5. Matusinovic, Z.; Wilkie, C. A. *J. Mater. Chem.* **2012**, *22*, 18701.
6. Paul, D. R.; Robeson, L. M. *Polymer* **2008**, *49*, 3187.
7. Wypych, F.; Satyanarayana, K. G. *J. Colloid Interface Sci.* **2005**, *285*, 532.
8. Wang, Q.; O'Hare, D. *Chem. Rev.* **2012**, *112*, 4124.
9. Manzi-Nshuti, C.; Songtipya, P.; Manias, E.; Jimenez-Gasco, M. M.; Hossenlopp, J. M.; Wilkie, C. A. *Polymer* **2009**, *50*, 3564.
10. Realinho, V.; Antunes, M.; Arenco, D.; Fernandez, A. I.; Velasco, J. I. *J. Appl. Polym. Sci.* **2009**, *111*, 2574.
11. Lonkar, S. P.; Morlat-Therias, S.; Caperaa, N.; Leroux, F.; Gardette, J. L.; Singh, R. P. *Polymer* **2009**, *50*, 1505.
12. Botan, R.; Nogueira, T. R.; Wypych, F.; Lona, L. M. F. *Polímeros* **2011**, *21*, 34.

13. Botan, R.; Nogueira, T. R.; Wypych, F.; Lona, L. M. F. *Polym. Eng. Sci.* **2012**, *52*, 1754.
14. Nyambo, C.; Songtipya, P.; Manias, E.; Jimenez-Gasco, M. M.; Wilkie, C. A. *J. Mater. Chem.* **2008**, *18*, 4827.
15. Nogueira, T.; Botan, R.; Wypych, F.; Lona, L. *Compos. A* **2011**, *42*, 1025.
16. Wang, L.; Su, S.; Chen, D.; Wilkie, C. A. *Polym. Degrad. Stab.* **2009**, *94*, 770.
17. Matusinovic, Z.; Feng, J.; Wilkie, C. A. *Polym. Degrad. Stab.* **2013**, *98*, 1515.
18. Nyambo, C.; Wang, D.; Wilkie, C. A. *Polym. Adv. Technol.* **2009**, *20*, 332.
19. Xu, Z. P.; Braterman, P. S.; Yu, K.; Xu, H.; Wang, Y.; Brinker, C. J. *Chem. Mater.* **2004**, *16*, 2750.
20. Xu, Z. P.; Braterman, P. S. *Appl. Clay Sci.* **2010**, *48*, 235.
21. Kuehn, T.; Porllmann, H. *Clays Clay Miner.* **2010**, *58*, 596.
22. Botan, R.; Gonçalves, N. A.; Moraes, S. B.; Lona, L. M. F. *Polímeros* **2015**, *25*, 117.
23. De Moraes, S. B.; Botan, R.; Lona, L. M. F. *Quim. Nova* **2014**, *37*, 18.
24. Qiu, L.; Chen, W.; Qu, B. *Colloid Polym. Sci.* **2005**, *283*, 1241.
25. Iyi, N.; Tamura, K.; Yamada, H. *J. Colloid Interface Sci.* **2009**, *340*, 67.
26. Nhlapo, N.; Motumi, T.; Landman, E.; Verryn, S. M. C.; Focke, W. W. *J. Mater. Sci.* **2008**, *43*, 1033.
27. Nogueira, T. R.; Lona, L. M. F.; Mcmanus, N. T.; Vivaldo-Lima, E.; Penlidis, A. J. *J. Mater. Sci.* **2010**, *45*, 1878.
28. American Society for Testing and Materials. In Annual Book of ASTM Standards; ASTM D 790-10; American Society for Testing and Materials: West Conshohocken, PA, **2010**.
29. Miyata, S.; Kumura, T. *Chem. Lett.* **1973**, *2*, 843.
30. Rives, V. Layered Double Hydroxide: Present and Future; Nova Science: New York, **2006**.
31. Depège, C.; El Metoui, F. Z.; Forano, C.; Roy, A.; Dupuis, J.; Besse, J. P. *Chem. Mater.* **2006**, *8*, 952.
32. Arizaga, G. G. C.; Mangrich, A. S.; Gardolinski, J. E. F. C.; Wypych, F. *J. Colloid Interface Sci.* **2008**, *320*, 168.
33. Nogueira, T.; Botan, R.; Neto, J. C. M.; Lona, L. *Adv. Polym. Technol.* **2013**, *32*, E660.
34. Manzi-Nshuti, C.; Chen, D.; Su, S.; Wilkie, C. A. *Polym. Degrad. Stab.* **2009**, *94*, 1290.
35. El-Bashir, S. *Polym. Bull.* **2013**, *70*, 2035.
36. Ayewah, D. O. O.; Davis, D. C.; Krishnamoorti, R.; Lagoudas, D. C.; Sue, H. J.; Willson, M. *Compos. A* **2010**, *41*, 842.
37. Nayak, S. K.; Mohanty, S. *J. Appl. Polym. Sci.* **2009**, *112*, 778.
38. Callister, W. D. Materials Science and Engineering: An Introduction; Wiley: New York, **2007**.
39. Grassi, V. G.; Forte, M. M. C.; Dal Pizzol, M. F. *Polím. Ciênc. Tecnol.* **2001**, *11*, 158.